Computational models of the neural control of breathing

4 authors, including:

Yaroslav I Molkov
Georgia State University
69 PUBLICATIONS **447** CITATIONS

Ilya A Rybak
Drexel University College of Medicine
72 PUBLICATIONS **2,551** CITATIONS

Computational models of the neural control of breathing

Yaroslav I. Molkov,[1][†] Jonathan E. Rubin,[2][†] Ilya A. Rybak[3][†],[*] and Jeffrey C. Smith[4][†]

The ongoing process of breathing underlies the gas exchange essential for mammalian life. Each respiratory cycle ensues from the activity of rhythmic neural circuits in the brainstem, shaped by various modulatory signals, including mechanoreceptor feedback sensitive to lung inflation and chemoreceptor feedback dependent on gas composition in blood and tissues. This paper reviews a variety of computational models designed to reproduce experimental findings related to the neural control of breathing and generate predictions for future experimental testing. The review starts from the description of the core respiratory network in the brainstem, representing the central pattern generator (CPG) responsible for producing rhythmic respiratory activity, and progresses to encompass additional complexities needed to simulate different metabolic challenges, closed-loop feedback control including the lungs, and interactions between the respiratory and autonomic nervous systems. The integrated models considered in this review share a common framework including a distributed CPG core network responsible for generating the baseline three-phase pattern of rhythmic neural activity underlying normal breathing. © 2016 Wiley Periodicals, Inc.

INTRODUCTION

The respiratory neural control system in mammals involves many interacting structures and dynamic biophysical processes operating at multiple spatial and temporal scales continuously throughout life. Breathing movements, which provide gas flow into and out of the lungs for homeostatic regulation of oxygen and carbon dioxide, are produced by neural networks in the central nervous system (CNS). These networks generate the rhythm of breathing and the spatiotemporal patterns of neural activity required to coordinate the complex movements of the peripheral respiratory apparatus for this homeostatic regulation. The processes involved at the level of neural cells and circuits are constantly regulated by afferent input signals from peripheral mechanosensory mechanisms and oxygen/carbon dioxide sensors located within and outside of the CNS. Understanding the integrated operation of this system is a fundamental, unsolved problem in respiratory physiology and neuroscience.

Computational modeling is becoming increasingly important in the endeavor to understand the dynamical operation of the respiratory control system.[1] In this review, we summarize recently developed models and analyze various aspects of the neural control of breathing at different levels of complexity. We start by considering models that focus on the dynamic operation of key brainstem neural networks involved in generating the normal pattern of breathing. Then, we move beyond this baseline function to more complicated models examining how activity of these networks is regulated by afferent signals that modify breathing behavior, as well as how

[†]These authors contributed equally.

[*]Correspondence to: rybak@drexel.edu

[1]Department of Mathematics and Statistics, Georgia State University, Atlanta, GA, USA

[2]Department of Mathematics, University of Pittsburgh, Pittsburgh, PA, USA

[3]Department of Neurobiology and Anatomy, Drexel University College of Medicine, Philadelphia, PA, USA

[4]Cellular and Systems Neurobiology Section, National Institute of Neurological Disorders and Stroke, National Institutes of Health, Bethesda, MD, USA

neural dynamics are coupled to peripheral gas exchange and transport for closed-loop control. Finally, a model of the interactions of the respiratory neural system with the autonomic nervous system is also described. In addition to providing a theoretical framework for analyzing the neurobiological processes involved, all of these models were developed to explain experimental observations and to generate predictions for subsequent experimental investigations. We therefore consider both the ability of these data-driven models to reproduce the experimentally observed behaviors and the mechanistic insights that the models provide.

MODELING THE BRAINSTEM RESPIRATORY CENTRAL PATTERN GENERATOR NETWORK

Network Organization and Neurophysiology

The rhythmic neural activity that produces breathing movements in mammals is generated by specialized neuronal networks—the respiratory central pattern generator (CPG)—located in the brainstem. This rhythmic activity emerges from the intrinsic biophysical properties of, and synaptic interactions between, neuronal populations involved in CPG operation that are spatially distributed within identified regions of the pons and medulla. A series of computational models has been developed to reproduce experimental data and provide explanations for neural processes and mechanisms operating in the CPG neurons and circuits. The activity patterns of brainstem respiratory neurons and the CNS efferent motor output during the respiratory cycle have been established experimentally from extensive electrophysiological recording studies (see Lindsey et al.[1] for a comprehensive review). Essential neurophysiological features that the models are designed to explain are summarized below.

During normal breathing, the rhythmic motor pattern consists of three neural activity 'phases': inspiration (I), post-inspiration (post-I or P-I) or the first stage of expiration, and the later or second stage of expiration (called E-2).[2,3] This basic three-phase motor pattern reflects the coordinated activity of numerous populations of brainstem and spinal motoneurons that are driven and controlled by the brainstem CPG circuits. These motor output neurons include cranial motoneurons in the brainstem controlling musculature of the upper airways (e.g., hypoglossal, glossopharyngeal, and laryngeal muscles) and motoneurons at the spinal cord level innervating muscles of the respiratory pump (diaphragm, thoracic intercostal, and abdominal musculature).

The CPG circuits that generate the three phases of the respiratory cycle are constructed from core sets of interacting populations of excitatory (glutamatergic) and inhibitory (glycinergic and/or GABAergic) interneurons whose activity is transmitted via mono- and polysynaptic circuits to the motoneurons. A central hypothesis in the field, supported by electrophysiological recordings, is that these key populations of interneurons are bilaterally distributed in three anatomically and functionally distinct compartments in the ventrolateral medulla (Figure 1(a)): the Bötzinger complex (BötC), pre-Bötzinger complex (pre-BötC), and rostral ventral respiratory group (rVRG). These compartments are components of a more extensive 'ventral respiratory column' (VRC) that is distributed rostrocaudally on each side of the brainstem and also includes more caudal (cVRG) and more rostral [retrotrapezoid nucleus (RTN) or parafacial respiratory group (pFRG)] regions.[4] The latter regions are also included in a series of models, which are discussed in detail in later sections. The BötC, pre-BötC, and rVRG contain neuron populations that are predominantly active with some temporal dispersion during the inspiratory phase (inspiratory or I-neurons) or during the post-I or E-2 expiratory phase (expiratory or E-neurons). Critical populations of inspiratory neurons are concentrated in the pre-BötC. These include populations of intrinsically rhythmogenic excitatory pre-I/I[1,4,5] (also called I-Driver[1,6]) and early-I[2,4,5] (or I-DEC[1,6,7]) neurons (see Table 1 and Figure 1(a) and (b) for nomenclature and activity profiles). The premotor inspiratory neurons (ramp-I[2,4,5] or I-AUG[1,6,7] types) are located in the rVRG. Populations of expiratory neurons are located more rostrally in the BötC (post-I[2,4,5] or E-DEC[1,6,7] neurons, as well as aug-E[4,5] or E-AUG[1,6,7] neurons that are active during the E-2 phase). This spatial distribution of neuron types suggests a specific compartmental organization of mechanisms producing inspiratory and expiratory activity. It is postulated that these populations form local microcircuits that interact within and between these compartments.[1,4–6]

The microcircuits of excitatory and inhibitory respiratory neurons within the pre-BötC and BötC are considered to be the core circuits of the CPG responsible for generating and controlling the three-phase respiratory pattern. Experimental data suggest that the BötC circuits are essential for generating expiratory activity and include populations of inhibitory neurons
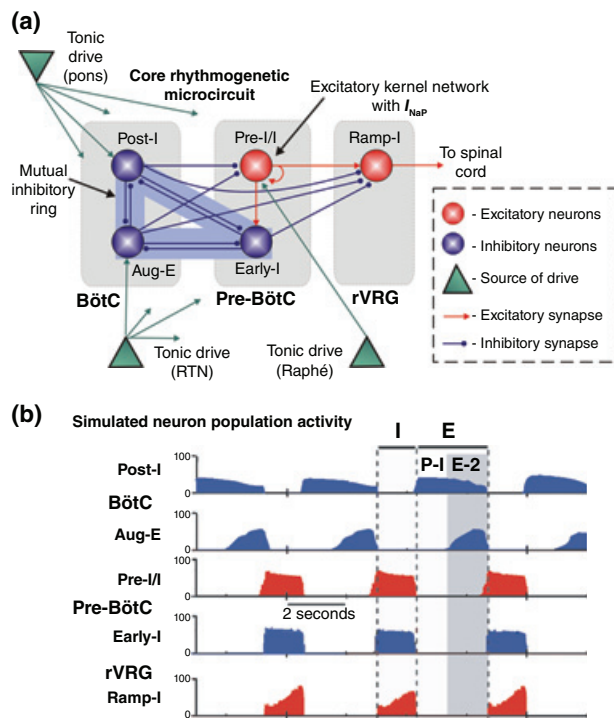
(a)

(b)

FIGURE 1 | Legend on next column.

active during the post-I and E-2 expiratory phases. The pre-BötC has bilaterally interacting excitatory circuits that constitute the critical inspiratory oscillator. These neurons have intrinsic cellular and circuit mechanisms for the generation of rhythmic inspiratory activity. Models of the biophysical bases of rhythmic bursting behavior of pre-BötC excitatory neurons and circuits, beginning with the models developed by Butera et al.[15,16] have incorporated a persistent sodium current (I_{NaP}) (and in some models, a calcium-activated nonspecific cation current, I_{CAN}[17-21]) defining the rhythmogenic properties of these neurons. Pre-BötC inhibitory interneurons that are active in the inspiratory phase (early-I neurons), driven locally by the excitatory neurons, are critical for coordinating activity of inspiratory and expiratory circuits. The pre-BötC rhythmogenic excitatory neurons drive excitatory neurons in the rVRG, which contains the main population of excitatory premotor bulbospinal inspiratory (ramp-I) neurons that project to phrenic and other spinal inspiratory motoneurons as well as cranial inspiratory motoneurons for generation of inspiratory motor outputs. Convergent inputs to the core pre-BötC and BötC circuits from other populations of brainstem interneurons (Figure 1(a)) are critical for generation of the normal three-phase respiratory pattern. These include tonic excitatory inputs from pontine circuits in the rostral

brainstem, specifically to the BötC, to control generation of the post-I activity phase. Excitatory inputs from the RTN/pFRG function as a major source of

TABLE 1 | Types of Neurons, Their Properties, and Dominant Location

Neuron Type	Other Names	Properties	Dominant Location
pre-I/I[4,5]	EI/I, I-Driver[1,6,7]	Excitatory neurons, with firing activity starting in late expiration and continuing throughout inspiration (could be intrinsically bursting)	pre-BötC
ramp-I[3–5]	I-AUG[1,6,7]	Excitatory neurons, active during inspiration with augmenting spike frequency within bursts	rVRG
early-I[3–5]	I-DEC[1,6,7]	Inhibitory neurons, active during inspiration with decrementing spike frequency within bursts	pre-BötC
post-I[3–5]	E-DEC[1,6,7]	Inhibitory neurons, active during expiration (or only during the initial post-inspiratory phase) with decrementing spike frequency within bursts	BötC, pre-BötC, cVRG
aug-E[4,5]	E-AUG,[1,6,7] E2[3]	Inhibitory neurons, active during expiration (or only during E2 phase) with augmenting spike frequency within bursts	BötC, cVRG
late-E[8,9]	pre-I[10–13]	Excitatory neurons active at the very end of expiration and not during inspiration (could be intrinsically bursting, could have a second active phase during post-inspiratory phase)	RTN/pFRG

BötC, Bötzinger complex; cVRG, caudal ventral respiratory group; pFRG, parafacial respiratory group; rVRG, rostral ventral respiratory group; RTN, retrotrapezoid nucleus.

chemosensory (CO_2/pH and O_2-related) drive and are involved in homeostatic regulation of respiration in response to various metabolic demands. Other brainstem sources of afferent input include the serotonergic raphé nuclei (also with CO_2 chemosensory properties) and the nuclei of the tractus solitarius (NTS), which also project to the RTN and pons, conveying mechanosensory signals and input from peripheral chemoreceptors sensing O_2.[4]

Computational Models of the Core CPG Circuits

Three types of neuronal models—conductance-based (Hodgkin–Huxley, HH, type), integrate-and-fire (IF), and activity-based models—have been developed to analyze the dynamic operation of the core circuits within the pre-BötC and BötC. These models attempt to explain, at different levels of neurobiological and computational complexity, how intrinsic neuronal biophysical mechanisms are combined with inhibitory and excitatory network interactions, including external excitatory inputs from pontine and RTN/pFRG circuits, to generate the three-phase respiratory pattern.

The conductance-based (HH-type[1,4,5,22,23]) and IF[1,6,7] models incorporate synaptically coupled populations of inspiratory and expiratory spiking single-compartment neurons. The neuronal membrane currents and conductances incorporated in HH neuron models[1,4,5,22,23] include action potential generating transient Na^+ and delayed rectifier K^+

currents, as well as a membrane leak current. The models for inhibitory early-I, post-I, and aug-E neurons also have ionic channels that orchestrate intrinsic spike frequency adaptation properties produced by Ca^{2+}-dependent K^+ currents activated by Ca^{2+} flux via high voltage-activated Ca^{2+} currents during neuronal spiking. This adaptation property assists in respiratory phase transitions. The pre-BötC pre-I/I excitatory neuron model incorporates I_{NaP}. The spiking IF models[1,6,7] do not include transient Na^+ and delayed rectifier K^+ currents and use simpler mathematical descriptions of spike generation and frequency adaptation. Populations of neurons, consisting of 50–200 cells for each type of inspiratory or expiratory neurons, are constructed with heterogeneity of neuronal excitability, implemented in the HH-type models by selecting some model biophysical parameters from random distributions. Excitatory and inhibitory synaptic interactions among populations are modeled by postsynaptic conductances in target neurons, activated by presynaptic spiking of neurons providing the activity-dependent synaptic inputs. The model circuitry is shown schematically in Figure 1(a) and includes tonic excitatory drives from the pons, RTN, and raphé nuclei to the neuronal microcircuits in the three major medullary compartments (BötC, pre-BötC, and rVRG). An example of activity of the simulated populations of HH neurons from this model is shown in Figure 1(b).

Model simulations have reproduced some essential temporal features of the three-phase

population activities and network outputs recorded in experimental rat brainstem-spinal cord preparations (e.g., see Smith et al.[5,22] for model-data comparisons). The model parameters chosen for simulations allowed the model to reproduce experimental data obtained from these preparations. A good model-data correspondence implies that the model architecture for the core pre-BötC and BötC circuits defines plausible interactions of the excitatory and inhibitory populations driving the generation of the three-phase respiratory pattern. The simulations show that the three-phase pattern can be explained by the dynamic interactions between (1) the reciprocally connected post-I and aug-E inhibitory populations in the BötC that are active during expiration, (2) the early-I inhibitory neuron population in the pre-BötC that is active during inspiration and suppresses activity of BötC neurons, and (3) the pre-I/I excitatory population in the pre-BötC that generates the inspiratory rhythm and is inhibited by synaptic inputs from the BötC neurons during the expiratory phases. In essence, the pre-BötC and BötC inhibitory neuron populations along with the specified sets of reciprocal inhibitory interconnections underlie the circuit interactions that coordinate inspiratory and expiratory phases (see Richter and Smith[24] for review). The excitatory pre-BötC circuits provide the neuronal biophysical and circuit mechanisms for generating rhythmic inspiratory activity.

Simulations with the neuronal population models based on the HH-type spiking neuron models have reproduced a number of experimental observations[1,4–6,22] including (1) perturbations of the frequency and amplitude of inspiratory activity following pharmacological suppression of I_{NaP}; (2) disruptions of network activity induced by reducing inhibitory synaptic interactions, consistent with the proposed role of inhibitory circuit interactions in three-phase pattern generation; and (3) reconfiguration of CPG network activity and changes in the rhythmogenic mechanisms and motor patterns following various brainstem transections that physically reduce the brainstem respiratory network. These simulations have delineated mechanistically how the core CPG components could be assembled from the postulated pre-BötC and BötC microcircuits and external excitatory drive inputs.

These simulations lead to a series of predictions concerning the anticipated changes in the breathing pattern following the general and/or site-specific suppression of inhibitory interactions within the pre-BötC and BötC. Some of these were tested and confirmed experimentally,[5,25] providing support for the suggested organization of neuronal interactions in these key respiratory compartments.

Activity-based (nonspiking) models of the core pre-BötC and BötC circuitry that incorporate the essential adaptation properties of inhibitory neurons and I_{NaP}-dependent intrinsic burst generation mechanisms of pre-BötC excitatory neurons in a more simplified mathematical format have been developed by Rubin et al.[8,26] These models have the same types of early-I, post-I, aug-E inhibitory neurons and pre-I/I excitatory neurons and the same circuit architecture of inhibitory and excitatory interactions as in the large-scale population models with the conductance-based neuron models. However, these simplified models have reduced parameter sets compared with the large-scale conductance-based models. Specifically, the dynamic behavior of each excitatory and inhibitory neuronal population is represented by mathematical formulations that define a type of activity profile analogous to the integrated activities shown in Figure 1(b). Therefore, these simplified models are particularly useful for establishing a minimal construct sufficient to produce the key dynamical processes represented in the complex large-scale conductance-based models. This approach has also allowed the use of analytical tools from dynamical systems theory including phase plane and bifurcation analyses to study in greater detail the dynamic mechanisms underlying transitions between respiratory phases.

The activity-based models have reproduced many of the experimental results described earlier. Simulations with these simplified models have generally shown that the basic architecture and key properties of the core pre-BötC and BötC circuits constitute a robust dynamical structure. The mutual inhibitory circuits interacting within and between the pre-BötC and BötC, and the interactions with the excitatory pre-I/I population, intrinsically give rise to stable phase transitions. This further supports the conclusion that the core circuit architecture represented in the two types of models is a plausible configuration for generating the three-phase respiratory pattern. These models have also shown how the different external excitatory drives acting on each excitatory or inhibitory population in the pre-BötC and BötC compartments can regulate the frequency and durations of inspiratory and expiratory phases and make predictions about effects of altered drives to particular components.[26] These results suggest that the proposed network architecture and compartmental organization allows flexible multi-level control of different circuit components for regulation of inspiratory and expiratory activities.[4]

BRAINSTEM RESPIRATORY NETWORK AND INTERACTING OSCILLATORS

Dual Oscillator Models

As described in the previous section, the current models of the core respiratory network operating within and between the pre-BötC and BötC can capture a wide range of experimentally observed phenomena. Nonetheless, there are other neuronal populations and circuit interactions that contribute to rhythmic respiratory pattern generation and control under different conditions. In particular, experimental studies have identified a neuronal population in the parafacial respiratory group (pFRG) located within or overlapping with the RTN, which is capable of autonomous rhythmic activity[10,11,27] involving I_{NaP}.[9] It has been suggested that this population represents the primary inspiratory oscillator[11,28] or an expiratory rhythm generator that interacts with the inspiratory oscillator in the pre-BötC.[12,13,29] Alternatively, there is evidence that pFRG oscillations are suppressed under normal conditions and are recruited to drive abdominal motor output when the respiratory system engages in active expiration, such as during exercise or hypercapnic conditions requiring a high level of lung ventilation.[12,14,30–37]

Several computational models have been developed specifically to explore the dual respiratory oscillator framework.[38–41] The earliest of these models simply represents each oscillator with an abstract, scalar ordinary differential equation.[38] In this framework, each oscillator is represented by a phase in $[0,2\pi)$, which is reset back to 0 when 2π is crossed, corresponding to the firing of a burst, and the oscillators are coupled in a phase-dependent way. Unfortunately, the lack of biological content in this model severely limits its utility for comparison with experimental findings and its predictive power.

The model by Wittmeier et al.[39] also consists of two synaptically coupled units represented by I_{NaP}-driven single neuron bursters[15] capable of generating periodic bursts of action potentials. In this model, the pre-BötC burster inhibits the pFRG burster, which in turn excites the pre-BötC burster. The basic model output consists of a periodic pattern, with each cycle composed of (1) a brief pre-inspiratory/late-expiratory pFRG burst, which is interrupted by (2) an inspiratory pre-BötC burst recruited by excitation from the pFRG, followed by (3) a longer, post-inspiratory/expiratory pFRG burst resulting from post-inhibitory rebound that arises from the removal of inhibition by the termination of the pre-BötC burst.

The pre-BötC burst itself terminates through the inactivation of I_{NaP}, without the need for any synaptic inputs. This overall output pattern emerges as long as the pre-BötC burst frequency is less than that of the pFRG, which would presumably be a prediction for experimental testing.

With these features, the model is capable of reproducing several experimental results, including experiments in which pFRG stimulation imposed sufficiently soon after the post-I phase yields a biphasic pFRG response and prolonged expiration phase, whereas later pFRG stimulation shortens the subsequent expiratory phase.[10,27,42] The model can also produce quantal slowing of pre-BötC activity, a phenomenon in which opioid-induced depression of the pre-BötC can cause pre-BötC activation to occur only once every n respiratory cycles for some integer n.[12] There are some serious issues with this model, however. One weakness relates to the model construction: to prevent an additional pre-BötC burst from interrupting the longer post-inspiratory pFRG burst, a tonic inhibitory signal is directly imposed on the pre-BötC neuron for the duration of this particular pFRG burst; no neural mechanism for this specifically timed arrival of inhibition is modeled or proposed. Furthermore, the model requires not just hyperpolarisation of the pre-BötC neuron but also the imposition of a stochastic reduction of synaptic excitation from the pFRG to the pre-BötC to produce the quantal slowing effect, which lacks biological justification.

The model by Lal et al.[40] in contrast to the others includes not just a pair of bursters but a collection of 81 I_{NaP}-based pacemaker neurons[15] in each of the pre-BötC and the pFRG. Like the previous model, the synaptic coupling from the pre-BötC to the pFRG is inhibitory while that from the pFRG to the pre-BötC is excitatory, with heterogeneous synaptic strengths. The model exhibits a baseline, periodic activity pattern very similar to that of the Wittmeier et al.[39] model, with each cycle featuring brief late-E and longer post-I pFRG activity periods sandwiching a pre-BötC burst. With variation of synaptic conductances, the model can also produce regimes with monophasic pFRG activation, which can either precede or occur in synchrony with each pre-BötC burst. A triumph of the model is the production of quantal slowing of the pre-BötC resulting solely from increased leak conductance, without suppression or stochasticity of synaptic connections, albeit with details depending sensitively on the distributions of other parameters in the model. The quantal slowing occurs because with decreased pre-BötC excitability, more synaptic inputs are needed to recruit a

synchronized pre-BötC population burst. On most cycles in this regime, only a fraction of pre-BötC neurons activate, and this is considered inadequate to drive an inspiratory output.

A fundamental problem with this model, as well as the others described so far, is that in the baseline activity regime, there is a complete pause in network activity between the post-inspiratory and late-expiratory/pre-inspiratory pFRG bursts. A related point is that the loss of late-E activity in these models would imply loss of post-I activity as well, since both activity phases are driven by the same pFRG oscillator. Importantly, recent experimental results cast doubt on the dual oscillator framework as a mechanism underlying normal inspiratory/expiratory alternation. In particular, experiments have shown that RTN/pFRG phasic activation drives abdominal motor output and, with the possible exception of neonatal animals, this output does not appear in the late-E phase during normocapnic expiration but rather arises specifically during active expiration associated with hypercapnia and other metabolic challenges.[9,30,31,34,41]

Incorporating the RTN/pFRG into the Brainstem Respiratory Network: Emergence of Late-E Oscillations

Recently, two computational models, one in the conductance-based[9] and one in the activity-based framework,[8] have been developed that capture metabolic state-dependent recruitment of RTN/pFRG activity, reproduce a variety of experimental findings beyond the scope of the earlier models, and, in the latter case, allow for dynamical systems analysis of the mechanisms underlying model behaviors. These models start from the framework of the basic CPG circuit (as shown in Figure 1) and add a late-E population in the RTN/pFRG (see Table 1), whose I_{NaP}-dependent bursting activity emerges during active expiration associated with certain metabolic challenges (see Figure 2(a)). Taking note of experimental findings that the lack of late-E bursts under normal conditions may stem from inhibition of chemosensitive RTN neurons by medullary CPG neurons,[43–45] the models include inhibition of the late-E population of the RTN/pFRG by both the post-I population of the BötC and the early-I population of the pre-BötC. In turn, these late-E neurons excite pre-I/I and aug-E neural populations and project to the cVRG to induce the late-E discharges in abdominal motoneurons as observed in recordings from the abdominal nerve (AbN) during active expiration (Figure 2(a)).

Experiments performed in an *in situ* perfused rat brainstem-spinal cord preparation[9] have also shown that progressive increase of CO_2 (increasing hypercapnia) leads to the quantal acceleration of late-E activity in the AbN with a gradual shift from late-E activation once every n ($n > 1$) respiratory cycles to late-E activation each cycle ($n = 1$) (Figure 2(b1)–(b4)). This mechanism has been reproduced in both models.[8,9] Because of the inhibition it receives in the models (Figure 2(a)), the late-E population remains silent in normocapnic, normoxic conditions. With an increase of CO_2 level this population receives an additional excitation from RTN. Due to this excitation, the late-E population in RTN/pFRG becomes rhythmically active and produces a burst of activity at the end of the expiratory phase of some respiratory cycles. Progressive augmentation of hypercapnia yields quantal acceleration of late-E activity until it eventually achieves activation in each respiratory cycle (Figure 2(c1)–(c4)).

The more complex large-scale conductance-based model also reproduces experimental observations[9,31,46] that the delay of phrenic nerve (PN) activation relative to hypoglossal nerve activation significantly increases in respiratory cycles featuring AbN activity. This result emerges by design in the model: late-E excitation of pre-I/I neurons promotes hypoglossal activation, while the early-I population that is excited by the late-E cells inhibits the neurons that drive PN activation.

Another agreement between models and experimental observations is that when hypoxia is modeled as a decrease in pontine drive to the medullary core CPG, the progressive induction of hypercapnic hypoxia yields a transition from monophasic to biphasic late-E bursts[9,10,12,27,28,31,33,47] (Figure 3(a) and (b)). Interestingly, simulations predict (Figure 3) that during the progressive development of hypoxia, there should be a transition from the regime where late-E activity is purely post-inspiratory to the regime characterized by biphasic late-E activity (Figure 3(b)), so that the pattern of late-E and abdominal activities (mono- or biphasic) depends on the level of oxygen. This prediction awaits experimental testing.

Finally, both models captured the finding that experimental administration of opioid agonists induced a quantal slowing of pre-BötC activity in which pre-BötC neurons only activate once every n respiratory cycles for some $n > 1$.[12,13,33] Also, both models predict that the suppression of inhibition in RTN/pFRG should evoke abdominal late-E discharges under normal (normocapnic) conditions. This prediction was subsequently confirmed experimentally.[9]
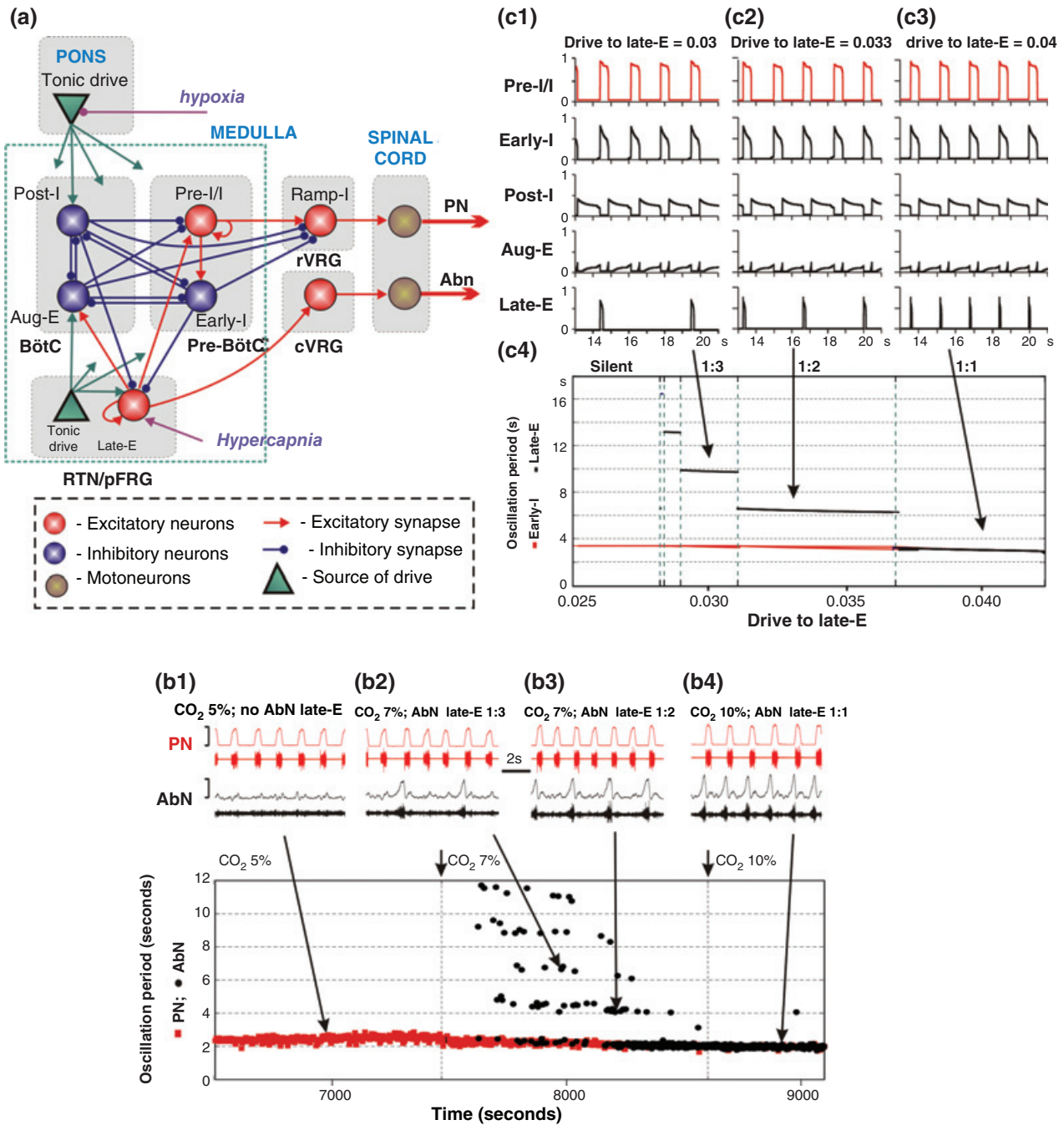
FIGURE 2 | Legend on next page.

Theoretical Investigation of Interactions Between Late-E and Pre-BötC Oscillations

Analysis of the nonspiking activity-based model,[8] using dynamical systems tools such as phase planes, provides additional mechanistic insight into the quantal acceleration of late-E neuronal activity with hypercapnia, the quantal slowing of pre-BötC activity with

opioid agonists, and the transformation of late-E activity from monophasic to post-inspiratory to biphasic with hypercapnic hypoxia.

First, consider quantal recruitment of late-E (Figure 2(c1)–(c4)). Because of the persistent sodium current of the late-E neuron,[9] its voltage (V) dynamics are bistable; that is, over a range of I_{NaP} inactivation (h) levels, V can be depolarized (with inactivation

increasing through the given level) or hyperpolarized (with inactivation decreasing). The full (V, h) dynamics has a resting equilibrium state, which lies on the hyperpolarized branch of the bistable range for baseline parameters. The bistable range of h and the equilibrium state both depend on the synaptic input to the late-E neuron, but throughout each respiratory cycle, although post-I activity wanes late within the expiratory phase, the hyperpolarized equilibrium state still remains. With hypercapnic excitatory drive to late-E, however, the waning of post-I inhibition can lower the bistable h range enough to eliminate the hyperpolarized equilibrium, which allows late-E to activate near the end of the post-I phase. Still more drive results in more lowering and allows late-E activation on more cycles, albeit always near the end of post-I; hence, quantal activation, phase-locked to post-I, results. Similar but more involved phase plane arguments can be used to show that since early-I activation in the model occurs in the face of augmenting aug-E inhibition even in the absence of late-E activity, the emergence of late-E activity has little effect on the timing of inspiratory onset. Indeed, even though late-E excites pre-I/I neurons, which in turn excite early-I neurons, the onset of early-I neuronal activity is underway before the early-I neurons are affected by late-E activity. Hence, as observed in the perfused brainstem-spinal cord experimental preparation (Figure 2(b, bottom)), late-E recruitment does not impact inspiratory period (Figure 2(c4)).

If pontine drive is also reduced in the hypercapnic state in which late-E activity occurs on each cycle, then post-I activity is reduced. We have already seen that the decay of post-I phase inhibition opens a window for late-E neuronal activation (Figure 3(b), left). A phase plane analysis can be used to show that the decay of a weaker inhibition allows this window to open earlier, and the immediate effect is that late-E activation transitions from late in the expiratory phase to earlier, within the post-I expiratory phase. When this transition first occurs, pre-I/I and early-I neurons are no longer ready to activate when late-E does, and hence there is a pause between late-E activation and inspiration (Figure 3(b), middle). However, this pause is not long enough to allow a second late-E activation. That situation changes with an additional hypoxia-induced reduction of pontine drive: weaker post-I neuronal output yields earlier late-E activation followed by late-E neuron recovery and re-activation. The latter occurs sufficiently later after inspiration to recruit pre-I/I and early-I neuronal activity despite strong aug-E inhibition, resulting in a biphasic regime with shortened period (Figure 3(b), right). Thus, like the previous model,[9] this model predicts that a regime of monophasic post-I activation of late-E neurons must occur before the transition to biphasic late-E activation with the progressive induction of hypercapnic hypoxia.

Finally, phase plane analysis is also useful for exploring opioid-induced quantal slowing of pre-BötC activity relative to late-E activity. Opioid effects are implemented in the model via a decrease in the excitatory synaptic conductances, corresponding to strengths of excitatory tonic drives, as well as connections from pre-I/I to early-I neuron and late-E to pre-I/I neuron. Phase planes can be used to show how the loss of excitation prevents pre-BötC neurons from activating between late-E and post-I on some

---

FIGURE 2 | Augmented respiratory central pattern generator (CPG) model produces experimentally observed quantal acceleration of late-E activity in hypercapnia. (a) Model schematic.[8,9] In addition to components shown in Figure 1(a), a late-E population with oscillatory capabilities supported by I_{NaP} is included. This population makes and receives a variety of synaptic connections as shown. In particular, it excites a caudal ventral respiratory group (cVRG) population that drives motor output via the abdominal nerve (AbN). Note that hypercapnia is implemented as an additional drive to the late-E population while hypoxia is simulated as a decrease in the output from the pons. In a perfused rat brainstem-spinal cord preparation, increased perfusate CO_2 yields quantal acceleration of late-E AbN activity. (b1)–(b4) Simultaneously recoded raw activity (bottom) and integrated activity (top) of phrenic nerve (PN) and AbN during normocapnia ((b1), 5% CO_2) characterized by the absence of activity in the AbN, and with the development of hypercapnia, during which the ratio between the AbN and PN frequencies steps from 1:3 to 1:2 ((b2), (b3); 7% CO_2) to 1:1 ((b4) 10% CO_2). (bottom) Oscillation periods in the PN (red squares) and AbN (black circles) shown as functions of time throughout the experiment. The AbN late-E bursts were phase-locked to the PN bursts with a ratio that increased quantally from 1:5 to 1:1. The CO_2 in the perfusate was changed at the times indicated by short arrows and vertical dashed lines. The episodes shown in (b1)–(b4) occurred at the times indicated by large arrows. (c1)–(c3) Increasing hypercapnic drive to the late-E neuron yields quantal acceleration of late-E activity in the activity-based, nonspiking model.[8] Outputs from model components at particular levels of hypercapnic drive show integer ratios of late-E activations to full respiratory cycles as well as phase-locking of late-E activity to occur at the transition between expiration and inspiration marked by decaying post-I activity and maximal aug-E activity. (c4) Analogously to the experimental results, the time courses of late-E (black dots) and early-I (red dots) periods (defined as durations between successive activations) show a quantal acceleration from 1:5 to 1:1 with progressive increases in drive to the late-E neuron, and the early-I period remains approximately constant throughout. Arrows indicate drive levels used in (c1)–(c3). (Figure 2(a) and (b1)–(b4, bottom)—Reprinted with permission from Ref 9. Copyright 2010; Figure 2(c1)–(c4)—Reprinted with permission from Ref 8. Copyright 2011)
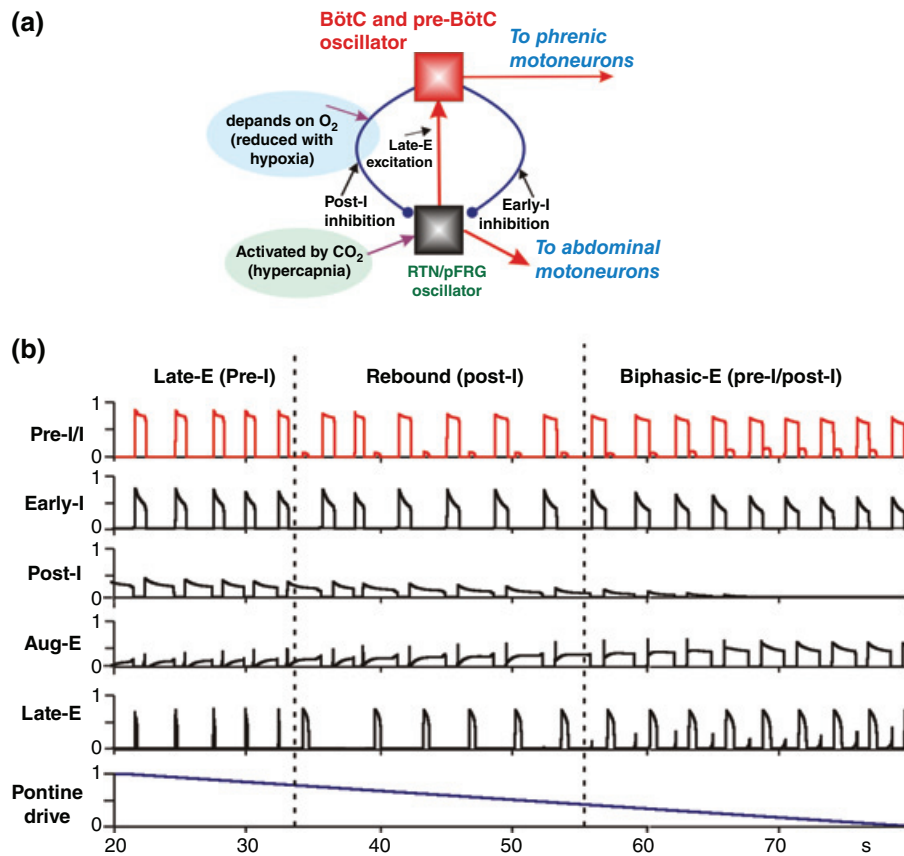
(a)

(b)

FIGURE 3 | Interactions between Bötzinger complex/pre-Bötzinger complex (BötC/pre-BötC) and retrotrapezoid nucleus/ parafacial respiratory group (RTN/pFRG) affect timing of late-E neuron activation in hypercapnia. (a) Lumped schematic illustration of the relation between the BötC/pre-BötC (encompassing pre-I/I, early-I, post-I, and aug-E populations) and RTN/pFRG components of the respiratory network. RTN/pFRG activity can be recruited by hypercapnia, implemented as a direct excitation in computational models, or by hypoxia, implemented as a reduction of pontine drive yielding an effective drop in post-I inhibitory output (maroon arrows). Red arrows denote excitatory pathways, while connections ending in circles represent inhibitory interactions. (Reprinted with permission from Ref 9. Copyright 2010) (b) In an activity-based, nonspiking computational model, starting from simulated hypercapnia with monophasic activation of RTN/pFRG (labeled as late-E on the y-axis) in the late-E phase of each respiratory cycle (compare late-E timing to pre-I, early-I, post-I, and aug-E), hypoxia simulated by progressive reduction of pontine drive (bottom) yields a gradual shift in the timing of RTN/pFRG activation. With partial reduction of drive, activation shifts to the post-I phase (middle), while additional loss of drive results in biphasic activation. Note as well the loss of post-I activity and change in aug-E activity profile with decreased drive. (Reprinted with permission from Ref 8. Copyright 2011)

cycles and renders the pre-BötC neurons dependent on excitation from late-E neurons in order to activate at all. Hence, the slowing is indeed quantal, locked to late-E activation. Perhaps most surprisingly, the model offers an explanation for why late-E activity is biphasic on precisely those cycles with pre-I/I and early-I neuron activation. Early-I inhibits late-E and hence cuts short its activity. This reduces the I_{NaP} inactivation in late-E neurons and allows them to rebound at the end of the inspiratory phase. Subsequently, there is enough time for late-E to recover and activate again with its usual late-expiratory timing. Importantly, both models predict that RTN/pFRG is needed to trigger pre-BötC activity in this scenario of reduced pre-BötC sensitivity to

inputs, unlike during the normal eupnoeic rhythm generation.

MODELING THE CLOSED-LOOP CONTROL OF BREATHING

Computational Models of Respiratory Network Controlling Lung Ventilation and Gas Exchange

Breathing subserves the vital process of gas exchange between the lungs and the air, which is provided by the rhythmic contraction of the diaphragm and other (abdominal and intercostal) muscles, which in turn are controlled by the corresponding motoneuron

pools. The activities of phrenic and abdominal moto-neurons represent major outputs of the brainstem respiratory CPG network. Most of the existing models of the closed-loop respiratory system[48–61] described this system at different levels of detail with a focus either on the neural controller and the respiratory CPG,[51,53,59,60] on lung mechanics,[58,60] or on gas exchange,[48,50,56,57] but usually without a unified consideration of all of these components. For example, Ben-Tal and Smith[56,57] proposed an integrated closed-loop model that included lung mechanics and gas exchange but used a significantly reduced description of the neural respiratory CPG and did not consider mechanical feedback from the lungs. Rybak et al.[53] and later Molkov et al.[59] developed and analyzed a model with a detailed description of the brainstem CPG connected to a very simple model of the lungs along with mechanical feedback to the respiratory network. These models could reproduce multiple experimental findings, including changes in the respiratory pattern following vagotomy and/or the suppression of pontine-medullary interactions. However, these models did not consider lung mechanics, gas exchange and transport and chemical feedback. Longobardo et al.[55] adapted previously developed models of the respiratory CPG and connected them to a neurochemical feedback model to control ventilation, but this model did not simulate lung mechanics. Finally, O'Connor et al.[60] developed a sophisticated computational model of the respiratory neural network focusing on the biomechanics of breathing and airway defensive behavior. This model included a detailed representation of the respiratory CPG connected with a well-elaborated biomechanical model of the lungs and upper airways. The objective of the study was to reproduce the respiratory motor pattern during eupnoeic breathing and its changes during several important motor behaviors, such as cough and swallowing. Although this model provided detailed descriptions of both the neural CPG and lung mechanics, it did not incorporate gas exchange and transport components and did not include chemical feedback to the respiratory network; hence, the model could not simulate respiratory system behavior during metabolic challenges, such as hypercapnia or hypoxia.

It is important to mention that the closed-loop models of breathing mentioned above focused on quiet (passive) breathing, during which the pumping of air in the lungs is mostly performed by the diaphragm, driven by phrenic motoneuronal output controlled by the CPG during inspiration. In such quiet breathing, thoracic intercostal and abdominal muscle contraction during expiration is minimal and does not play a significant role in ventilation. These models do not capture the forced or active expiration, which can arise during intense exercise or severe hypercapnia[62–66] and involves activation of abdominal muscles to provide a forced expulsion of the air from the lungs during expiration. As described in the previous section, the transition from quiet breathing to breathing with active or forced expiration is characterized by the emergence of rhythmic activity in the RTN/pFRG. The emergence of RTN/pFRG oscillations is accompanied by well-expressed pre-inspiratory (pre-I) or late-expiratory (late-E) discharges in the abdominal motor output that appear at the end of expiration just before inspiratory bursts seen in the PN.[9,12,31,32] However, the models discussed above do not consider the role of abdominal late-E discharges in the framework of the closed-loop respiratory control system and how these discharges affect ventilation.

To investigate control of breathing during active expiration, Molkov et al.[67] developed a closed-loop computational model of the respiratory system that includes the elaborated model of the brainstem respiratory CPG network driving lung ventilation and gas exchange. This model allows simulation of breathing regimes with passive and active expiration and transitions between them. The schematic of the model is shown in Figure 4. The brainstem respiratory network is based on the activity-based models of the respiratory CPG developed by Rubin et al.,[8,26] which as described in the previous section, represent reduced versions of the preceding large-scale models.[5,9,22,53] Similar to the previous CPG models, this model incorporates interactions between the inhibitory network of the post-I, aug-E, and early-I neurons and the excitatory pre-I/I neurons. The behavior of this network depends on excitatory drives from the pons and RTN/pFRG. Interactions between the late-E neurons of the RTN/pFRG and the core circuit neurons in the BötC and pre-BötC follow the circuit organization proposed in previous studies[8,9,31] (see the previous section).

The lung and gas exchange sub-systems are based on the earlier models of Ben-Tal and Smith.[56,57,68] The lungs are represented as a single container. In contrast to the original models by Ben-Tal and Smith, which contain only one pump simulating the effects of diaphragm contraction, this model contains two pumps, one representing the diaphragm and the other simulating the effects of abdominal muscle contraction (Figure 4). Both the diaphragm and abdominal muscles are modeled as springs, whose lengths are controlled by the external
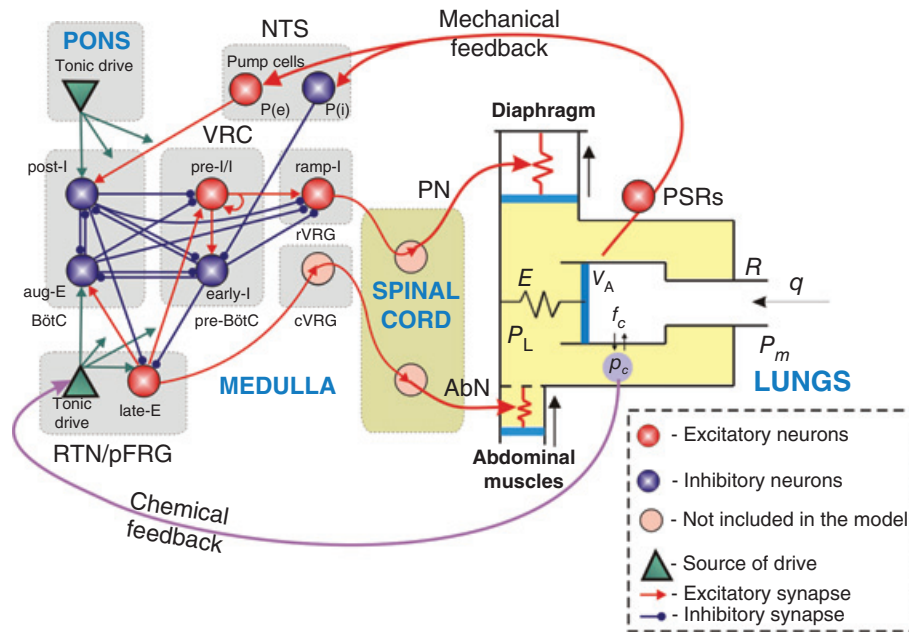
FIGURE 4 | Schematic of the closed-loop respiratory system model. AbN, abdominal nerve; aug-E, augmenting expiratory neuron; BötC, Bötzinger complex; cVRG, caudal ventral respiratory group; early-I, early-inspiratory neuron; late-E, late-expiratory neuron; NTS, nucleus of the tractus solitarius; P(e), excitatory pump cells; P(i), inhibitory pump cells; pFRG, parafacial respiratory group; PN, phrenic nerve; post-I, post-inspiratory neuron; pre-BötC, pre-Bötzinger complex; pre-I/I, pre-inspiratory/inspiratory neuron; PSRs, pulmonary stretch receptors; ramp-I, ramp-inspiratory neuron; RTN, retrotrapezoid nucleus; rVRG, rostral ventral respiratory group; VRC, ventral respiratory column. (Reprinted with permission from Ref 67. Copyright 2014)

forces defined by the activities of the PN or AbN, respectively.

To simplify gas exchange and transport in the model, it was assumed that the volume of the capillaries is the same as the heart stroke volume and that the transit time of blood through the lung is the same as the time interval between heartbeats. Movement of blood through the lungs is simulated by re-initializing the values of blood partial pressures of carbon dioxide and oxygen on each heart beat (for more details see Ben-Tal[68]). The heart is modeled as a pump that at every heartbeat instantaneously delivers a portion of the venous blood with preset partial pressures of oxygen and carbon dioxide. Between heartbeats, these pressures are adjusted due to diffusion between the blood and lung alveoli.

The model includes two types of feedback, mechanical and chemical. The mechanical feedback is provided by signals from pulmonary stretch receptors (PSRs), which respond to lung inflation. The mechanical feedback signal is defined by the excess of lung volume above the functional residual capacity during inspiration and is considered to be zero when the lung volume is below the functional residual capacity. The mechanical feedback signal, conveyed to the brainstem respiratory CPG via the excitatory (P(e)) and inhibitory (P(i)) pump cells (P-cells) of the

NTS, excites the post-I neuron and inhibits the early-I neuron (Figure 4). Since the lung volume increases during inspiration, mechanical feedback promotes an advanced termination of the inspiratory phase and increases of breathing frequency. Vagotomy is modeled as the removal of mechanical feedback, achieved by setting PSR activity to zero.

Chemical feedback in the model includes only central chemoreception and is provided via the CO_2–dependent increase of tonic excitatory drive from the RTN to the respiratory network, including the late-E neuron within the RTN/pFRG (Figure 4). An increase in the RTN drive affects the activity of the rVRG ramp-I neuron and thus amplifies the phrenic motor output, which increases the maximal lung volume. To a minor extent RTN output also modulates the frequency of breathing.

The Molkov et al.[67] model generates the typical activity patterns of respiratory neurons, including an augmenting firing profile of the ramp-I neuron (and the PN output). Under normal (i.e., normocapnic) conditions, tonic drive to the late-E neuron of the RTN/pFRG is relatively weak and this neuron remains silent. Correspondingly, the AbN is not active under normal conditions. Passive breathing occurs due to contraction of the diaphragm and the corresponding lung inflation during inspiration (with

an increase in the lung volume V_A) produced by rhythmic PN activation.

The duration and amplitude of inspiratory activity and the frequency of respiratory oscillations are controlled by the mechanical feedback representing the so-called Hering–Breuer (HB) reflex.[69–71] The HB reflex operates in the model due to activation of PSRs during lung inflation, which (via NTS pump cells) excites the post-I neuron and inhibits the early-I neuron (see Figure 4), thereby promoting the termination of inspiration. The model is able to simulate vagotomy (removal of mechanical feedback) associated with the loss of the HB reflex leading to a prolongation of inspiration, an increase in the amplitude of PN activity and lung inflation (maximal lung volume), and a deceleration of respiratory oscillations, which all are consistent with experimental data.[69,72] Removal of pontine drive in the model after simulated vagotomy leads to an apneustic breathing pattern characterized by a significant increase in the duration of inspiration and a reduction of oscillation frequency. These features are typical for apneusis observed in experimental animals.[65,69,71,73]

Modeling Hypercapnia and Breathing with Active Expiration

As shown in many physiological studies, hypercapnia causes an increase of ventilation. Ventilation is enhanced due to increases in both the amplitude (lung tidal volume) and the rate of breathing (respiratory frequency), at least when vagal feedback is intact.[66,69,74–76] With the progressive development of hypercapnia (increase of CO_2 levels in blood and tissue), as described in the previous section, the respiratory system undergoes a transition from passive expiration typical for quiet breathing to breathing with active or forced expiration that involves recruitment of abdominal muscles contributing to pumping air out of the lungs.[62–64]

Similar to the previous models[8,9,31] described earlier, the late-E discharges in the Molkov et al.[67] model are generated by the late-E neuron located in the RTN/pFRG (see Figure 4). This neuron is activated during hypercapnia when it receives sufficient excitatory drive from the RTN. The emerging late-E discharges couple with and are phase-locked to phrenic discharges. With the progressive development of hypercapnia the system goes through quantal acceleration[9] until a 1:1 regime is attained, in which each PN discharge is preceded by a late-E (and AbN) discharge (see the previous section, Figure 2(b)). Hypercapnia is simulated as an increase in the value of a CO_2 concentration parameter f_{cm} ($f_{cm} = 0$ –

10% with $f_{cm} = 0$ representing normocapnia). The f_{cm} level affects gas exchange dynamics and defines the arterial CO_2 partial pressure, which in turn determines the CO_2-dependent RTN drive to both the VRC respiratory network and the late-E neuron within the RTN/pFRG (Figure 4). With a progressive increase of hypercapnia from $f_{cm} = 0$ to $f_{cm} = 10\%$ (gray triangle at the bottom of Figure 5(a)), late-E discharges (indicated by the left vertical dot-dashed line) first appear at about $f_{cm} = 2.6\%$ (see also Figure 5(b)), while the regime with a 1:1 ratio of late-E to PN discharges is reached at the level of $f_{cm} = 7.2$ (Figure 5(b)). In addition to causing quantal recruitment of late-E and AbN activity, a hypercapnic increase in RTN drive to the VRC respiratory network increases the amplitude and frequency of phrenic output and, correspondingly, the amplitude (maximal value) and frequency of lung inflation.

Each pulse of late-E activity, representing the activity of the AbN, actuates the abdominal pump (Figure 4) to augment the exhalation of air from the lungs by reducing the basal (residual) level of the lung volume (see V_A trace in Figure 5(a)), providing an additional increase of tidal volume and ventilation relative to those observed in simulations without active expiration. Specifically, Figure 5(b) illustrates how tidal volume, breathing rate, and ventilation change relative to baseline levels (normocapnia) with the progressive development of hypercapnia (f_{cm} increase from 0 to 10%). To visualize the role of active expiration, the changes of all three major characteristics (tidal volume, breathing rate, and ventilation) that would occur without active expiration (represented by setting AbN = 0) are shown by the corresponding dashed lines. The additional increase of ventilation (relative to passive ventilation without involvement of the late-E/AbN activity) results mainly from an increase of tidal volume, reflecting the amplitude of breathing, rather than from an acceleration of breathing frequency. Indeed, the increase in breathing rate with the development of hypercapnia is smaller with active expiration than with passive breathing (Figure 5(b)). These conclusions are consistent with multiple experimental findings indicating that an increase in ventilation during hypercapnia occurs mostly due to an increase in the breathing amplitude and that the respiratory rate does not significantly increase with hypercapnia[66,69,74–76]

In summary, this modeling study predicts that the closed-loop respiratory control system switches to active or forced expiration when further increases of ventilation via increases in the rate and amplitude of breathing become insufficient for providing gas
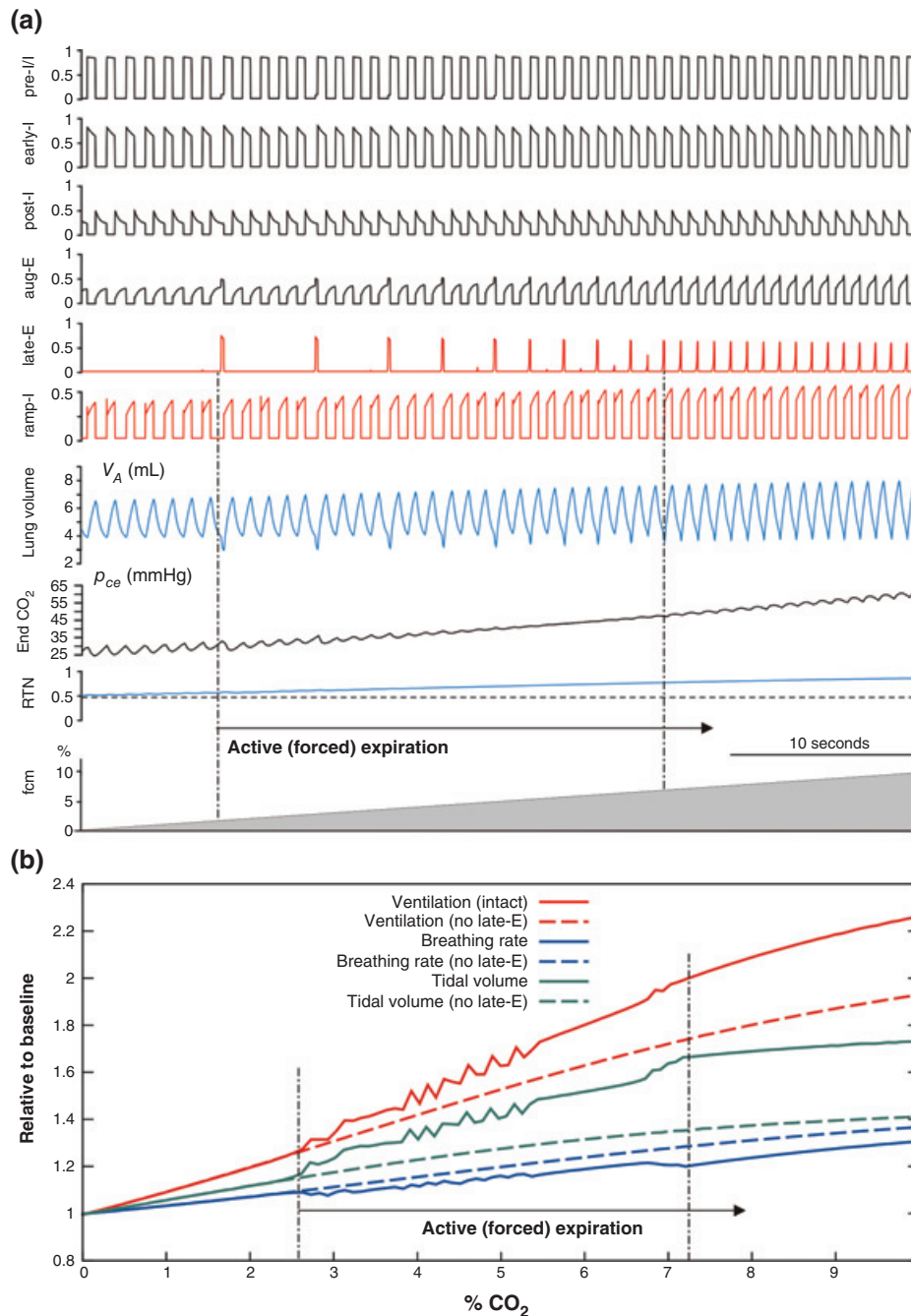

FIGURE 5 | Simulation of progressive hypercapnia with the closed-loop respiratory system model. (a) Model performance. The top 6 traces represent output activity (normalized firing rate) of the corresponding neurons. The bottom two traces represent the end capillary blood p_c (p_{ce}) just before the next heartbeat and the retrotrapezoid nucleus (RTN) drive, respectively. The continuous increase of hypercapnia (the gray ramp at the bottom) was induced by increasing CO_2 content in the mouth (f_{cm}) from 0 to 10%. Active expiration starts with the first appearance of late-E discharges (indicated by the left vertical dot-dashed line at f_{cm} = 2.6%) and reaches the regime with a 1:1 ratio of late-E to ramp-I activations at f_{cm} = 7.2% (right dot-dashed line). As described in the text, each late-E discharge, representing the activity of abdominal nerve (AbN) output, actuates the abdominal pump that reduces the baseline level of lung volume (see in the V_A trace). (b) Changes in tidal volume, breathing rate, and ventilation (relative to normocapnia) with the development of hypercapnia. CO_2 content in the mouth f_{cm} was linearly increased from 0 to 10%. Changes in three major breathing characteristics (tidal volume, breathing rate, and ventilation) that would occur without active expiration (simulated by setting AbN = 0) are shown by the corresponding dashed lines. The vertical dot-dashed lines bound the development (quantal acceleration) of active expiration. (Reprinted with permission from Ref 67. Copyright 2014)
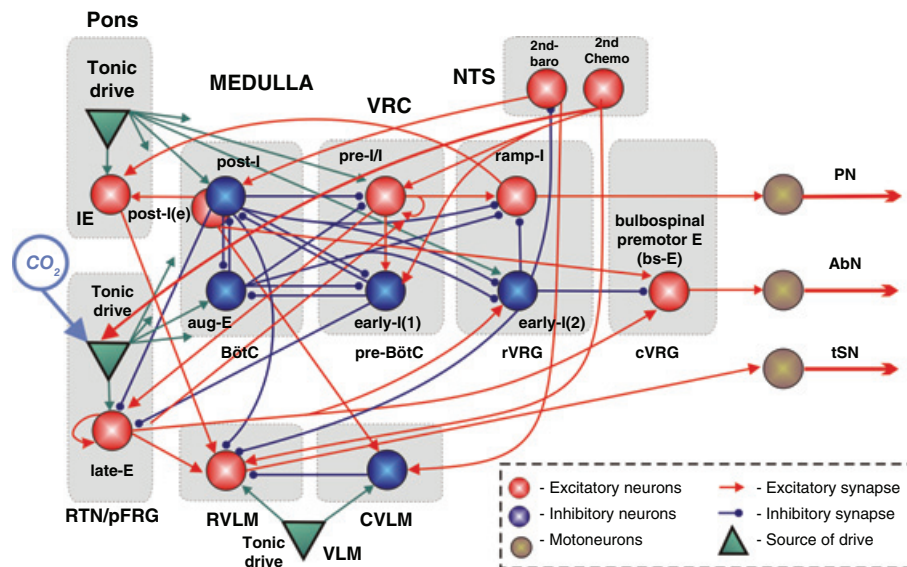
FIGURE 6 | Respiratory-autonomic system interactions. A network diagram representing a combination of models from Baekey et al.[83] and Barnett et al.[80] An excitatory population in the rostral ventrolateral medulla (RVLM) is a pre-sympathetic population receiving inputs from various respiratory populations that mediate respiratory modulation in the thoracic sympathetic nerve (tSN). Second order baroreceptors in the nucleus of solitary tract (NTS) project to a population of GABAergic neurons in the caudal ventrolateral medulla (CVLM), which in turn inhibit presympathetic RVLM neurons (classical baroreflex). In addition, NTS baroreceptors excite post-I neurons in Bötzinger complex (BötC, respiratory baroreflex). Second order peripheral chemoreceptors in the NTS excite pre-BötC pre-I/I neurons (providing an increase in respiratory frequency), central chemoreceptors in the retrotrapezoid nucleus [RTN, emergence of late-E activity in the abdominal nerve (AbN) and tSN], and premotor post-I population in the cVRG (not shown).

homeostasis in the blood and associated tissue. In such cases, the control system automatically activates the abdominal pump controlled by the late-E activity emerging in the RTN/pFRG, which provides additional exhalation of air from the lungs by reducing the minimal lung volume.

INTERACTIONS OF THE RESPIRATORY NETWORK WITH THE AUTONOMIC NERVOUS SYSTEM

Respiratory Modulation of Sympathetic Activity

Possible interactions between the respiratory CPG and autonomic nervous system drew a great deal of attention after correlations were found between obstructive sleep apnoea (OSA), arterial hypertension, sustained sympathetic overactivity, and peripheral chemoreflex activation.[77] In OSA, upper airways recurrently collapse during sleep leading to episodes of hypoxia. In rats, exposure to chronic intermittent hypoxia (CIH) results in long-term changes in baseline respiratory and sympathetic motor outflows.[78] Specifically, CIH rats demonstrate an active expiratory pattern with strong discharges at the end of expiration (late-E activity) even at normal CO_2

levels.[36] Simultaneous late-E bursts were observed in sympathetic activity,[36,78] which gave rise to the idea that CIH-induced neuroplasticity in the respiratory neuronal network is responsible for increased sympathetic activity and hypertension in OSA.[79,80]

It is known that respiratory neurons modulate the activity of pre-sympathetic neurons in the ventrolateral medulla,[81] which results in respiratory oscillations in the sympathetic motor outflow.[82] These oscillations were found to dramatically attenuate after ponto-medullary transection, which created a basis for a number of models featuring respiratory modulation of sympathetic nerve activity (SNA).[36,79,83,84]

In these models, baseline (normocapnic) respiratory modulation in SNA is provided by excitatory projections from phase-spanning inspiratory-expiratory neurons in the pons, and inhibitory projections from post-I and early-I neurons in the VRC to the excitatory pre-sympathetic population in the rostral ventrolateral medulla (RVLM) (Figure 6). Together these inputs create positive inspiratory modulation of the SNA. In hypercapnia, the same RVLM population receives additional excitatory input from the RTN/pFRG late-E population, which accounts for the emergence of late-E discharges in the AbN and the appearance of novel late-E bursts in the SNA.
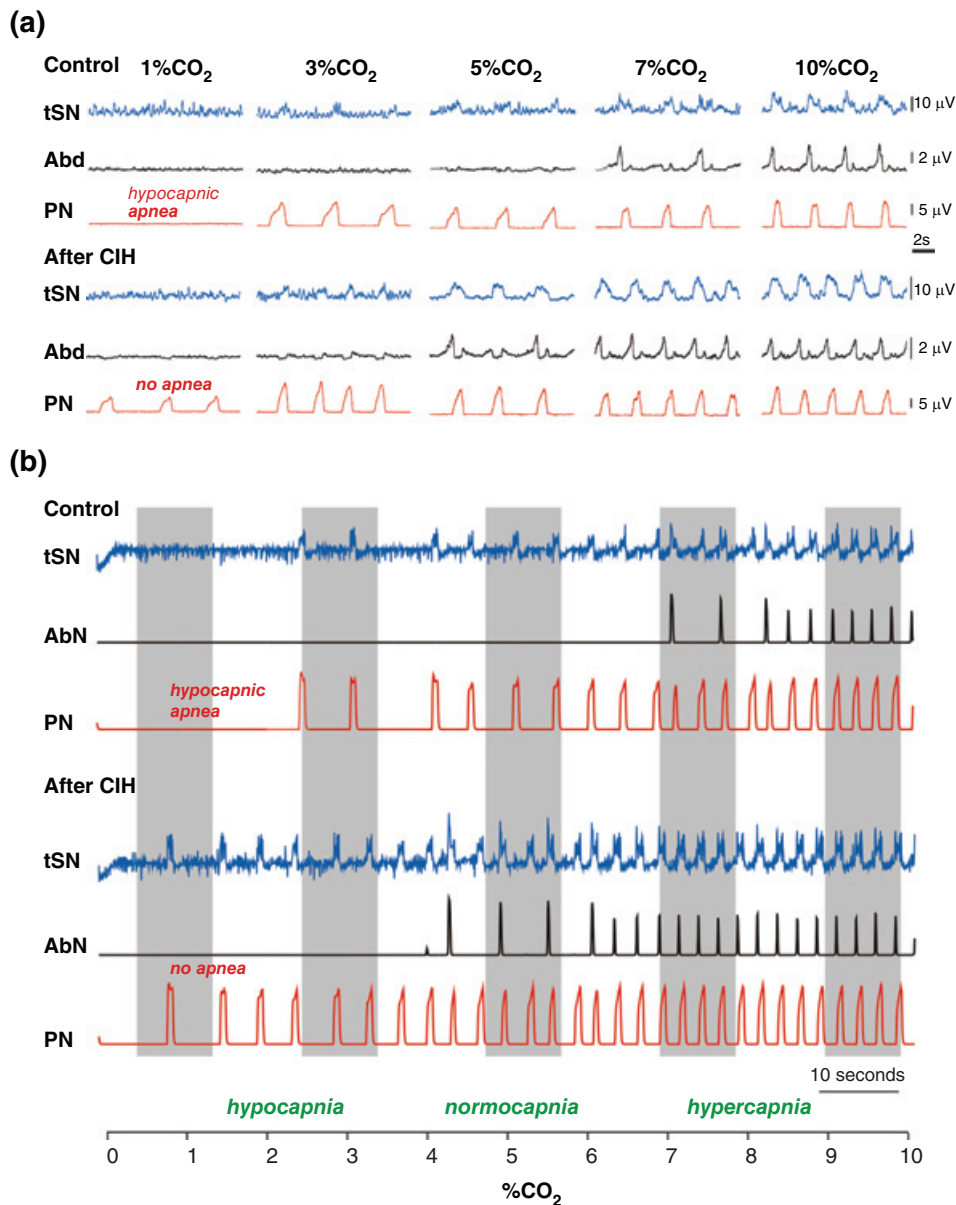
FIGURE 7 | Central chemoreflex. (a) Experimental recordings of respiratory (abdominal and phrenic) and sympathetic motor outputs in an in situ arterially perfused rat brainstem-spinal cord preparation at different CO_2 levels in the perfusate. (b) Simulations of progressive change in CO_2 content from hypocapnia to hypercapnia in the control model and the CIH model. Note hypocapnic shifts (toward lower CO_2 levels) produce changes in the emergence of late-expiratory activity in the abdominal nerve (AbN), and in the onset of respiratory activity of the phrenic nerve (PN, apneic threshold) in the CIH model. CIH, chronic intermittent hypoxia; tSN, thoracic sympathetic nerve. (Reprinted with permission from Ref 37. Copyright 2012)

The abdominal late-E activity arising at normal CO_2 levels after CIH exposure[78] can be abolished by hypocapnia (low CO_2 levels).[36] Together these findings suggest that CIH sensitizes central chemoreceptors, so that after CIH conditioning the respiratory drive from the RTN appears stronger at all CO_2 levels (Figure 7).[36,79,84] The mechanism of this sensitization was questioned by Barnett et al.[80] who hypothesized that increased excitability of the pFRG late-E

population results from stronger excitatory input from the pre-BötC pre-I/I population, and not from chemosensitive neurons in the RTN. This idea suggests that the direct consequence of CIH might be an elevation in the excitability of the excitatory pre-I/I population in the pre-BötC. Interestingly, these very neurons were found to have increased excitability due to lowered leak conductance in spontaneously hypertensive rats,[85] which contributed to the sympathetic

overactivity in these animals.[86] It still remains to confirm experimentally that the same mechanism is involved in a CIH-induced sympathetic excess.

Peripheral Chemoreflex

The role of the respiratory neural controller is to adjust ventilation in response to oxygen and carbon dioxide deviations from normal levels. In addition to the central chemoreceptors in the RTN mostly sensing CO_2 concentration, there are peripheral chemoreceptors located in the carotid bodies primarily responding to variations of oxygen concentration in the arterial blood. Peripheral chemoreceptors can be selectively activated by an injection of cyanides at low concentration[87] in the arterially perfused *in situ* rat brainstem-spinal cord preparation.[88] Barnett et al.[80] used such an approach to study the effects of peripheral chemoreceptors on respiratory and sympathetic motor outputs. They found that during peripheral chemoreflex activation, the respiratory frequency significantly increased, and motor patterns were profoundly altered. In particular, central vagus, hypoglossal, abdominal, and thoracic sympathetic nerves had a novel powerful post-inspiratory component in their activity pattern. In addition, abdominal and hypoglossal nerves exhibited late-expiratory discharges very similar to the ones observed during hypercapnia.[9,31]

To account for the changes in the respiratory frequency and pattern induced by peripheral chemoreceptor stimulation, Barnett et al.[80] produced an extended model incorporating second order relay neurons in the NTS activated by carotid body input and proposed a corresponding set of interconnections with respiratory and sympathetic neurons (Figure 6). They hypothesized that an increase in respiratory frequency during peripheral chemoreflex activation is mediated by direct projections from the NTS neurons to inspiratory neurons of the pre-BötC. The emergence of the late-E bursts in the AbN and SNA were explained by excitatory connections from the NTS neurons to a population of central chemoreceptors in the RTN, which in turn activate the pFRG late-E population. To accommodate the appearance of a post-inspiratory component in the respiratory motor outputs, they posited a novel bulbospinal post-I population in the cVRG, activated by peripheral chemoreceptor input from the NTS, and sending excitation to the hypoglossal, central vagus, and AbN motor outputs (not shown in Figure 6).

One of the interesting implications of this model is that during peripheral chemoreceptor activation, the pre-I/I population in the pre-BötC receives strong excitation through multiple pathways. First, it is directly excited by NTS neurons activated by peripheral hemoreceptors. Second, it also receives higher drive from the RTN central chemoreceptors driven by the peripheral chemoreflex. Barnett et al.[80] conjectured that repetitive excessive excitation of pre-I/I neurons during hypoxic episodes of CIH conditioning may underlie the resulting plasticity of channel expression. They suggested that an increase in pre-I/I excitability may be mediated by
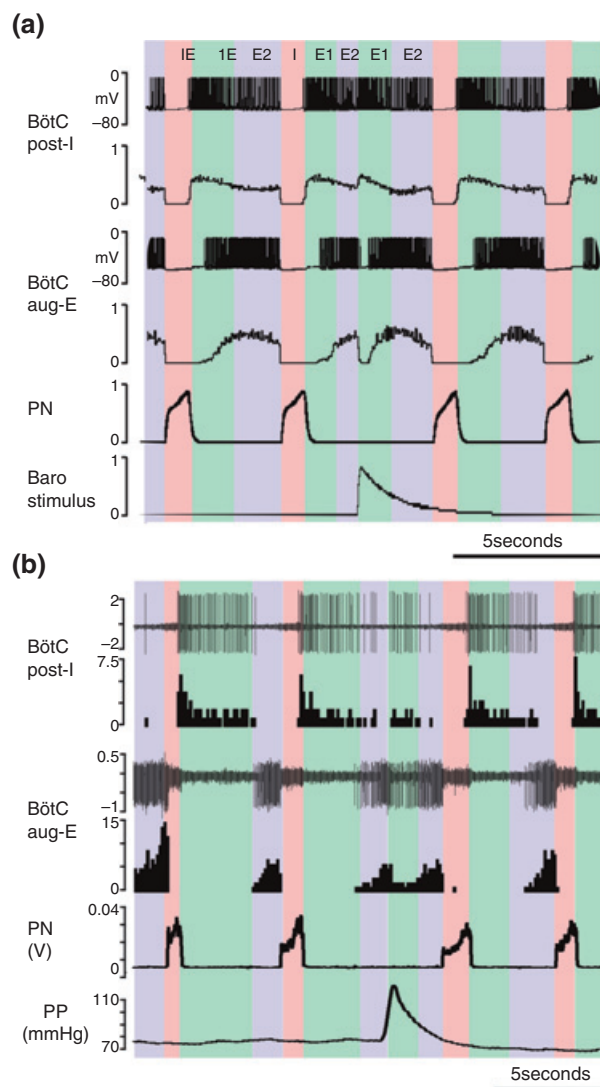
FIGURE 8 | Respiratory baroreflex. Expiration resetting by transient baroreceptor stimulation simulated in the Baekey et al.[83] model (a) and as experimentally recorded in situ (b). In (a), barostimulus activates the post-I population, which inhibits aug-E neurons. After the stimulus ends, the aug-E neurons activate for the second time. (b) Shows corresponding extracellular recordings and firing rate histograms from post-I and aug-E neurons in the BötC. (Reprinted with permission from Ref 83. Copyright 2010)

down-regulation of certain types of potassium channels in this population.

Respiratory Baroreflex

The interactions between respiratory and autonomic systems are bi-directional. Dick and Morris[89] demonstrated that a majority of respiratory neurons respond to transient arterial pressure pulses. It was further found that the activity of expiratory neurons is strongly affected by variations of arterial pressure,[90] which may have a profound effect on the duration of expiration. Baekey et al.[83] systematically studied the response of the respiratory CPG to transient pressure pulses by recording respiratory motor outflows and also the activity of individual cells. They found that short-lasting baroreceptor stimulation led to prolongation of the expiratory phase of CPG activity during which it was applied. Furthermore, the later in expiration the stimulus arrived, the stronger was the effect. They also observed that after ponto-medullary transection, baroreceptor stimulation did not have any influence on the duration of expiration, which led them to hypothesize that baroreceptor input primarily affects activity of the pontine-dependent post-I population of the CPG (Figure 6). This hypothesis was implemented as excitatory projections from second order baroreceptor cells in the NTS to the BötC post-I population in the extended model of the respiratory CPG.[79,83,84,91] The simulations revealed a complex dynamical mechanism of the CPG phase response to transient barostimulation: if the stimulus arrives in early expiration, i.e. during the post-I phase of the cycle, it has little effect on the pattern, as post-I neurons are strongly active. However, during the E-2 phase, the excitatory baroinput to post-I neurons significantly increases their firing rate and thus inhibits the activity of the aug-E neurons (Figure 8(a)). Once the stimulation ends, aug-E neurons activate again, preventing the start of the subsequent inspiratory burst. Baekey et al.[83] experimentally confirmed this scenario by multi-electrode single unit extracellular recordings from the BötC (Figure 8(b)).

An interesting prediction from this study is that the sympathetic baroreflex operates through multiple neuronal pathways including the ones mediated by respiratory neurons. The classical baroreceptor control of sympathetic activity is provided by the excitatory influence of NTS baroreceptor relay neurons on GABAergic neurons in the CVLM (Figure 6).[92] These neurons inhibit pre-sympathetic neurons in the RVLM thus lowering their activity and the sympathetic tone.[93,94] This pathway serves as a negative feedback suppressing fluctuations of the arterial pressure.[91] The above modeling study suggests that the respiratory modulation of sympathetic activity in combination with inputs that the respiratory CPG receives from baroreceptors via the NTS contributes to the sympathetic baroreflex response in a respiratory cycle phase-dependent manner.

CONCLUSION

Although the models reviewed above provide a sophisticated description of respiratory neuronal circuits, and their major sensory inputs and motor outputs, allowing them to reproduce a quite broad range of experimental findings, most of the detailed intrinsic properties and interconnections of the neurons in these models have not been directly and unequivocally established experimentally. Nonetheless, computational modeling of the brainstem networks involved in respiratory neural control has been instrumental in shaping the field of respiratory neurophysiology by formulating predictions and providing competing theoretical concepts for experimental testing. Novel experimental approaches, such as optogenetic manipulations, will provide access to populations of neurons in a manner highly specific to their location and mechanism of neurotransmission, which will challenge the models and thus serve as a basis for their further development

REFERENCES

1. Lindsey BG, Rybak IA, Smith JC. Computational models and emergent properties of respiratory neural networks. *Compr Physiol* 2012, 2:1619–1670.

2. Richter DW. Neural regulation of respiration: rhythmogenesis and afferent control. In: Greger R, Windhorst U, eds. *Comprehensive Human Physiology*, vol. 2. Berlin: Springer-Verlag; 1996, 2079–2095.

3. Richter DW, Spyer KM. Studying rhythmogenesis of breathing: comparison of in vivo and in vitro models. *Trends Neurosci* 2001, 24:464–472.

4. Smith JC, Abdala AP, Borgmann A, Rybak IA, Paton JF. Brainstem respiratory networks: building blocks and microcircuits. *Trends Neurosci* 2013, 36:152–162.

5. Smith JC, Abdala AP, Koizumi H, Rybak IA, Paton JF. Spatial and functional architecture of the mammalian brain stem respiratory network: a hierarchy of three oscillatory mechanisms. *J Neurophysiol* 2007, 98:3370–3387.

6. Rybak IA, O'Connor R, Ross A, Shevtsova NA, Nuding SC, Segers LS, Shannon R, Dick TE, Dunin-Barkowski WL, Orem JM, et al. Reconfiguration of the pontomedullary respiratory network: a computational modeling study with coordinated in vivo experiments. *J Neurophysiol* 2008, 100:1770–1799.

7. Balis UJ, Morris KF, Koleski J, Lindsey BG. Simulations of a ventrolateral medullary neural-network for respiratory rhythmogenesis inferred from spike train cross-correlation. *Biol Cybern* 1994, 70:311–327.

8. Rubin JE, Bacak BJ, Molkov YI, Shevtsova NA, Smith JC, Rybak IA. Interacting oscillations in neural control of breathing: modeling and qualitative analysis. *J Comput Neurosci* 2011, 30:607–632.

9. Molkov YI, Abdala AP, Bacak BJ, Smith JC, Paton JF, Rybak IA. Late-expiratory activity: emergence and interactions with the respiratory CPG. *J Neurophysiol* 2010, 104:2713–2729.

10. Onimaru H, Homma I. Respiratory rhythm generator neurons in medulla of brainstem-spinal cord preparation from newborn rat. *Brain Res* 1987, 403:380–384.

11. Onimaru H, Homma I. A novel functional neuron group for respiratory rhythm generation in the ventral medulla. *J Neurosci* 2003, 23:1478–1486.

12. Janczewski WA, Feldman JL. Distinct rhythm generators for inspiration and expiration in the juvenile rat. *J Physiol (Lond)* 2006, 570:407–420.

13. Mellen NM, Janczewski WA, Bocchiaro CM, Feldman JL. Opioid-induced quantal slowing reveals dual networks for respiratory rhythm generation. *Neuron* 2003, 37:821–826.

14. Smith JC, Abdala AP, Rybak IA, Paton JF. Structural and functional architecture of respiratory networks in the mammalian brainstem. *Philos Trans R Soc Lond B Biol Sci* 2009, 364:2577–2587.

15. Butera RJ, Rinzel J, Smith JC. Models of respiratory rhythm generation in the pre-Botzinger complex. I. Bursting pacemaker neurons. *J Neurophysiol* 1999, 82:382–397.

16. Butera RJ, Rinzel J, Smith JC. Models of respiratory rhythm generation in the pre-Botzinger complex. II. Populations of coupled pacemaker neurons. *J Neurophysiol* 1999, 82:398–415.

17. Rubin JE, Hayes JA, Mendenhall JL, Del Negro CA. Calcium-activated nonspecific cation current and synaptic depression promote network-dependent burst oscillations. *Proc Natl Acad Sci USA* 2009, 106:2939–2944.

18. Dunmyre JR, Del Negro CA, Rubin JE. Interactions of persistent sodium and calcium-activated nonspecific cationic currents yield dynamically distinct bursting regimes in a model of respiratory neurons. *J Comput Neurosci* 2011, 31:305–328.

19. Toporikova N, Butera RJ. Two types of independent bursting mechanisms in inspiratory neurons: an integrative model. *J Comput Neurosci* 2011, 30:515–528.

20. Jasinski PE, Molkov YI, Shevtsova NA, Smith JC, Rybak IA. Sodium and calcium mechanisms of rhythmic bursting in excitatory neural networks of the pre-Botzinger complex: a computational modelling study. *Eur J Neurosci* 2013, 37:212–230.

21. Park C, Rubin JE. Cooperation of intrinsic bursting and calcium oscillations underlying activity patterns of model pre-Botzinger complex neurons. *J Comput Neurosci* 2013, 34:345–366.

22. Rybak IA, Abdala AP, Markin SN, Paton JF, Smith JC. Spatial organization and state-dependent mechanisms for respiratory rhythm and pattern generation. *Prog Brain Res* 2007, 165:201–220.

23. Rybak IA, Smith JC. Computational modeling of the respiratory network. In: Binder MD, Hirokawa N, Windhorst U, eds. *Encyclopedia of Neuroscience*. Berlin/Heidelberg: Springer; 2009, 824–832.

24. Richter DW, Smith JC. Respiratory rhythm generation in vivo. *Physiology* 2014, 29:58–71.

25. Marchenko V, Koizumi H, Mosher B, Koshiya N, Tariq MF, Bezdudnaya TG, Zhang R, Molkov YI, Rybak IA, Smith JC. Perturbations of respiratory rhythm and pattern by disrupting synaptic inhibition within pre-Bötzinger and Bötzinger complexes. *eNeuro* 2016, 3. pii: ENEURO.0011-16.

26. Rubin JE, Shevtsova NA, Ermentrout GB, Smith JC, Rybak IA. Multiple rhythmic states in a model of the respiratory central pattern generator. *J Neurophysiol* 2009, 101:2146–2165.

27. Onimaru H, Arata A, Homma I. Primary respiratory rhythm generator in the medulla of brainstem-spinal cord preparation from newborn rat. *Brain Res* 1988, 445:314–324.

28. Onimaru H, Kumagawa Y, Homma I. Respiration-related rhythmic activity in the rostral medulla of newborn rats. *J Neurophysiol* 2006, 96:55–61.

29. Tupal S, Huang WH, Picardo MC, Ling GY, Del Negro CA, Zoghbi HY, Gray PA. Atoh1-dependent rhombic lip neurons are required for temporal delay between independent respiratory oscillators in embryonic mice. *Elife* 2014, 3:e02265.

30. Abbott SB, Stornetta RL, Fortuna MG, Depuy SD, West GH, Harris TE, Guyenet PG. Photostimulation of retrotrapezoid nucleus phox2b-expressing neurons in vivo produces long-lasting activation of breathing in rats. *J Neurosci* 2009, 29:5806–5819.

31. Abdala AP, Rybak IA, Smith JC, Paton JF. Abdominal expiratory activity in the rat brainstem-spinal cord in situ: patterns, origins and implications for respiratory rhythm generation. *J Physiol* 2009, 587:3539–3559.

32. Feldman JL, Del Negro CA. Looking for inspiration: new perspectives on respiratory rhythm. *Nat Rev Neurosci* 2006, 7:232–242.

33. Janczewski WA, Onimaru H, Homma I, Feldman JL. Opioid-resistant respiratory pathway from the preinspiratory neurones to abdominal muscles: in vivo and in vitro study in the newborn rat. *J Physiol* 2002, 545:1017–1026.

34. Guyenet PG, Mulkey DK. Retrotrapezoid nucleus and parafacial respiratory group. *Respir Physiol Neurobiol* 2010, 173:244–255.

35. Pagliardini S, Janczewski WA, Tan W, Dickson CT, Deisseroth K, Feldman JL. Active expiration induced by excitation of ventral medulla in adult anesthetized rats. *J Neurosci* 2011, 31:2895–2905.

36. Molkov YI, Zoccal DB, Moraes DJ, Paton JF, Machado BH, Rybak IA. Intermittent hypoxia-induced sensitization of central chemoreceptors contributes to sympathetic nerve activity during late expiration in rats. *J Neurophysiol* 2011, 105:3080–3091.

37. Rybak IA, Molkov YI, Paton JFR, Abdala APL, Zoccal DB. Modeling the autonomic nervous system. In: Robertson D, Biaggioni I, Burnstock G, Low P, eds. *Primer on the Autonomic Nervous System*. 3 ed. San Diego, CA: Elsevier; 2012, 681–687.

38. Joseph IM, Butera RJ. A simple model of dynamic interactions between respiratory centers. *Conf Proc IEEE Eng Med Biol Soc* 2005, 6:5840–5842.

39. Wittmeier S, Song G, Duffin J, Poon CS. Pacemakers handshake synchronization mechanism of mammalian respiratory rhythmogenesis. *Proc Natl Acad Sci USA* 2008, 105:18000–18005.

40. Lal A, Oku Y, Hulsmann S, Okada Y, Miwakeichi F, Kawai S, Tamura Y, Ishiguro M. Dual oscillator model of the respiratory neuronal network generating quantal slowing of respiratory rhythm. *J Comput Neurosci* 2011, 30:225–240.

41. Molkov Y. Coupled oscillations in neural control of breathing. In: *Encyclopedia of Computational Neuroscience*. New York, NY: Springer; 2015, 910–914.

42. Onimaru H, Arata A, Homma I. Localization of respiratory rhythm-generating neurons in the medulla of brainstem-spinal cord preparations from newborn rats. *Neurosci Lett* 1987, 78:151–155.

43. Fortuna MG, West GH, Stornetta RL, Guyenet PG. Botzinger expiratory-augmenting neurons and the parafacial respiratory group. *J Neurosci* 2008, 28:2506–2515.

44. Guyenet PG, Mulkey DK, Stornetta RL, Bayliss DA. Regulation of ventral surface chemoreceptors by the central respiratory pattern generator. *J Neurosi* 2005, 25:8938–8947.

45. Guyenet PG, Stornetta RL, Bayliss DA. Retrotrapezoid nucleus and central chemoreception. *J Physiol* 2008, 586:2043–2048.

46. Fukuda Y, Honda Y. Modification by chemical stimuli of temporal difference in the onset of inspiratory activity between vagal (superior laryngeal) or hypoglossal and phrenic nerves of the rat. *Jpn J Physiol* 1988, 38:309–319.

47. Onimaru H, Arata A, Homma I. Intrinsic burst generation of preinspiratory neurons in the medulla of brainstem-spinal cord preparations isolated from newborn rats. *Exp Brain Res* 1995, 106:57–68.

48. Grodins FS, Buell J, Bart AJ. Mathematical analysis and digital simulation of the respiratory control system. *J Appl Physiol* 1967, 22:260–276.

49. Eldridge F. The North Carolina respiratory model. In: *Bioengineering Approaches to Pulmonary Physiology and Medicine*. New York: Plenum Press; 1996, 25–49.

50. Lu K, Clark JWJ, Ghorbel FH, Ware DL, Zwischenberger JB, Bidani A. Whole-body gas exchange in human predicted by a cardiopulmonary model. *Cardiovascular Eng: An Inter J* 2003, 3:1–19.

51. Rybak IA, Paton JF, Schwaber JS. Modeling neural mechanisms for genesis of respiratory rhythm and pattern. II. Network models of the central respiratory pattern generato. *J Neurophysiol* 1997, 77:2007–2026.

52. Ursino M, Magosso E, Avanzolini G. An integrated model of the human ventilatory control system: the response to hypercapnia. *Clin Physiol* 2001, 21:447–464.

53. Rybak IA, Shevtsova NA, Paton JF, Dick TE, St-John WM, Morschel M, Dutschmann M. Modeling the ponto-medullary respiratory network. *Respir Physiol Neurobiol* 2004, 143:307–319.

54. Topor ZL, Pawlicki M, Remmers JE. A computational model of the human respiratory control system: responses to hypoxia and hypercapnia. *Ann Biomed Eng* 2004, 32:1530–1545.

55. Longobardo G, Evangelisti CJ, Cherniack NS. Introduction of respiratory pattern generators into models

of respiratory control. *Respir Physiol Neurobiol* 2005, 148:285–301.

56. Ben-Tal A, Smith JC. A model for control of breathing in mammals: coupling neural dynamics to peripheral gas exchange and transport. *J Theor Biol* 2008, 251:480–497.

57. Ben-Tal A, Smith JC. Control of breathing: two types of delays studied in an integrated model of the respiratory system. *Respir Physiol Neurobiol* 2010, 170:103–112.

58. Cheng L, Ivanova O, Fan HH, Khoo MC. An integrative model of respiratory and cardiovascular control in sleep-disordered breathing. *Respir Physiol Neurobiol* 2010, 174:4–28.

59. Molkov YI, Bacak BJ, Dick TE, Rybak IA. Control of breathing by interacting pontine and pulmonary feedback loops. *Front Neural Circuits* 2013, 7:16.

60. O'Connor R, Segers LS, Morris KF, Nuding SC, Pitts T, Bolser DC, Davenport PW, Lindsey BG. A joint computational respiratory neural network-biomechanical model for breathing and airway defensive behaviors. *Front Physiol* 2012, 3:264.

61. Ben-Tal A, Tawhai MH. Integrative approaches for modeling regulation and function of the respiratory system. *Wiley Interdiscip Rev Syst Biol Med* 2013, 5:687–699.

62. De Troyer A, Gilmartin JJ, Ninane V. Abdominal muscle use during breathing in unanesthetized dogs. *J Appl Physiol* 1989, 66:20–27.

63. Aliverti A, Cala SJ, Duranti R, Ferrigno G, Kenyon CM, Pedotti A, Scano G, Sliwinski P, Macklem PT, Yan S. Human respiratory muscle actions and control during exercise. *J Appl Physiol* 1997, 83:1256–1269.

64. West JB. *Respiratory Physiology: The Essentials*. Baltimore, MD: Wolters Kluwer Health/Lippincott Williams & Wilkins; 2008.

65. St-John WM. Neurogenesis of patterns of automatic ventilatory activity. *Prog Neurobiol* 1998, 56:97–117.

66. Saetta M, Mortola JP. Interaction of hypoxic and hypercapnic stimuli on breathing pattern in the newborn rat. *J Appl Physiol* 1987, 62:506–512.

67. Molkov YI, Shevtsova NA, Park C, Ben-Tal A, Smith JC, Rubin JE, Rybak IA. A closed-loop model of the respiratory system: focus on hypercapnia and active expiration. *PLoS One* 2014, 9:e109894.

68. Ben-Tal A. Simplified models for gas exchange in the human lungs. *J Theor Biol* 2006, 238:474–495.

69. Cohen MI. Neurogenesis of respiratory rhythm in the mammal. *Physiol Rev* 1979, 59:1105–1173.

70. Clark FJ, von Euler C. On the regulation of depth and rate of breathing. *J Physiol* 1972, 222:267–295.

71. Jodkowski JS, Coles SK, Dick TE. A 'pneumotaxic centre' in rats. *Neurosci Lett* 1994, 172:67–72.

72. Hayashi F, Coles SK, McCrimmon DR. Respiratory neurons mediating the Breuer-Hering reflex prolongation of expiration in rat. *J Neurosci* 1996, 16:6526–6536.

73. Morrison SF, Cravo SL, Wilfehrt HM. Pontine lesions produce apneusis in the rat. *Brain Res* 1994, 652:83–86.

74. Zhou D, Huang Q, Fung ML, Li A, Darnall RA, Nattie EE, St John WM. Phrenic response to hypercapnia in the unanesthetized, decerebrate, newborn rat. *Respir Physiol* 1996, 104:11–22.

75. Abu-Shaweesh JM, Dreshaj IA, Thomas AJ, Haxhiu MA, Strohl KP, Martin RJ. Changes in respiratory timing induced by hypercapnia in maturing rats. *J Appl Physiol* 1999, 87:484–490.

76. Tin C, Song G, Poon CS. Hypercapnia attenuates inspiratory amplitude and expiratory time responsiveness to hypoxia in vagotomized and vagal-intact rats. *Respir Physiol Neurobiol* 2012, 181:79–87.

77. Narkiewicz K, van de Borne PJ, Montano N, Dyken ME, Phillips BG, Somers VK. Contribution of tonic chemoreflex activation to sympathetic activity and blood pressure in patients with obstructive sleep apnea. *Circulation* 1998, 97:943–945.

78. Zoccal DB, Simms AE, Bonagamba LG, Braga VA, Pickering AE, Paton JF, Machado BH. Increased sympathetic outflow in juvenile rats submitted to chronic intermittent hypoxia correlates with enhanced expiratory activity. *J Physiol* 2008, 586:3253–3265.

79. Molkov YI, Zoccal DB, Baekey DM, Abdala AP, Machado BH, Dick TE, Paton JF, Rybak IA. Physiological and pathophysiological interactions between the respiratory central pattern generator and the sympathetic nervous system. *Prog Brain Res* 2014, 212:1–23.

80. Barnett WH, Abdala AP, Paton JF, Rybak IA, Zoccal DB, Molkov YI. Chemoreception and neuroplasticity in respiratory circuits. *Exp Neurol* 2017, 287:153–164.

81. Mandel DA, Schreihofer AM. Central respiratory modulation of barosensitive neurones in rat caudal ventrolateral medulla. *J Physiol* 2006, 572:881–896.

82. Baekey DM, Dick TE, Paton JF. Pontomedullary transection attenuates central respiratory modulation of sympathetic discharge, heart rate and the baroreceptor reflex in the in situ rat preparation. *Exp Physiol* 2008, 93:803–816.

83. Baekey DM, Molkov YI, Paton JF, Rybak IA, Dick TE. Effect of baroreceptor stimulation on the respiratory pattern: insights into respiratory-sympathetic interactions. *Respir Physiol Neurobiol* 2010, 174:135–145.

84. Rybak IA, Molkov YI, Paton JFR, Abdala APL, Zoccal DB. Modeling the autonomic nervous system. In: David R, Italo B, Geoffrey B, Phillip AL, Julian FRP, eds. *Primer on the Autonomic Nervous System*. San Diego: Academic Press; 2012, 681–687.

85. Moraes DJ, Machado BH, Paton JF. Specific respiratory neuron types have increased excitability that drive presympathetic neurones in neurogenic hypertension. *Hypertension* 2014, 63:1309–1318.

86. Moraes DJ, Machado BH, Paton JF. Carotid body overactivity induces respiratory neurone channelopathy contributing to neurogenic hypertension. *J Physiol* 2015, 593:3055–3063.

87. Costa-Silva JH, Zoccal DB, Machado BH. Glutamatergic antagonism in the NTS decreases post-inspiratory drive and changes phrenic and sympathetic coupling during chemoreflex activation. *J Neurophysiol* 2010, 103:2095–2106.

88. Paton JF. A working heart-brainstem preparation of the mouse. *J Neurosci Methods* 1996, 65:63–68.

89. Dick TE, Morris KF. Quantitative analysis of cardiovascular modulation in respiratory neural activity. *J Physiol* 2004, 556:959–970.

90. Dick TE, Shannon R, Lindsey BG, Nuding SC, Segers LS, Baekey DM, Morris KF. Arterial pulse modulated activity is expressed in respiratory neural output. *J Appl Physiol* 2005, 99:691–698.

91. Molkov Y. Baroreflex models. In: *Encyclopedia of Computational Neuroscience*. New York: Springer; 2015, 307–315.

92. Schreihofer AM, Guyenet PG. The baroreflex and beyond: control of sympathetic vasomotor tone by GABAergic neurons in the ventrolateral medulla. *Clin Exp Pharmacol Physiol* 2002, 29:514–521.

93. Dampney RA. Functional organization of central pathways regulating the cardiovascular system. *Physiol Rev* 1994, 74:323–364.

94. Loewy AD, Spyer KM. *Central Regulation of Autonomic Functions*. New York: Oxford University Press; 1990.